Engineering Structures

Magnetic flux leakage technique to detect loss in metallic area in external post-tensioning systems

Madhu M. Karthik[a,*], Tevfik Terzioglu[b], Stefan Hurlebaus[c], Mary Beth Hueste[c], Herbert Weischedel[d], Ronald Stamm[d]

[a] Civil Engineering, Indian Institute of Technology, Palakkad 678557, India
[b] Texas A&M Transportation Institute, College Station, TX 77843-3136, USA
[c] Zachry Department of Civil and Environmental Engineering, Texas A&M Univ., TX 77843-3136, USA
[d] NDT Technologies, Inc., P.O. Box 637, 345 Nutmeg Road South, South Windsor, CT 06074, USA

ARTICLE INFO

ABSTRACT

Post-tensioned girders with internal and external tendons are widely used for the construction of bridges because of their eminent advantages. However, owing to poor grout quality, damage to protective ducts, exposure to environmental conditions, overstressing of strands, and overloading of the girder, the external tendons are susceptible to corrosion and breakage of strands. It is important to identify loss in cross-sectional area of the strands, in order to take preventive actions to avoid loss in capacity, and in some cases even failure of the tendon. Magnetic Flux Leakage (MFL), a non-destructive evaluation technique, is used to detect and quantify metallic defects in external post-tensioning systems. In order to evaluate this technique in in-service bridges under field conditions, a full-scale post-tensioned girder specimen was constructed as a control specimen. Metal defects that include section loss, corrosion, and breakage in wire and single or multiple strands with known loss in cross-sectional area, were fabricated and placed in the external tendons. The MFL device is then used to evaluate loss in metallic area (LMA) in the control girder specimen. The MFL device consistently detects LMA greater than 5% of the total strand cross-sectional area for the group of strands in a tendon. The measurements are found to be repeatable and reproducible. Even though there are errors associated with the estimated LMA percentages, especially for defects with greater than 50% loss in cross-sectional area, the estimated magnitude of the loss in total strand cross-sectional area gives a good indication about the severity of the defect.

1. Introduction

Post-tensioning (PT) systems have enabled significant advancements in bridge engineering, and provide a safe and efficient construction solution for transportation infrastructure. PT systems can be effectively used to construct long span, aesthetically pleasing and economical structures with increased structural capacity and durability compared to conventional reinforced concrete structures. Owing to the inherent advantages of the PT systems, they are used to construct bridges quite often, especially when the cost of the substructure can be significant due to complexities in the location of the structure, such as bridges spanning water ways, valleys, or urban areas. PT systems are also used for rehabilitation and strengthening of existing bridges. Based on the location of the tendons in the cross-section of the girder, PT systems are classified as internal and external post-tensioning systems. The PT ducts are usually grouted, which acts as the corrosion protection

system. Due to absence of the protective cover concrete, and the possible presence of undesirable voids or grout defects, external tendons are more vulnerable to corrosion than internal tendons, even when exposed to similar environmental conditions.

Failure of post-tensioning systems of in-service bridges have occurred in the past [1–6]. A majority of these failures are associated with poor grout quality and/or poor grouting practices, which result in voids in the anchorage regions or along the PT system ducts. The presence of moisture in these voided regions leads to corrosion of the steel strands. Even though the quality of the grouting materials and construction practices have improved over the past decade, some existing post-tensioned bridge structures exhibit considerable degree of defects in the PT systems. Unlike corrosion of conventionally reinforced concrete systems where corrosion distress can be identified by discoloration/stains, cracking, or spalling of cover concrete, corrosion of PT strands is hidden and seldom show surface distress. Typically, the degree of corrosion of

---

post-tensioned strands is more critical to the structural performance than conventionally reinforced concrete systems. In the absence of timely inspection, maintenance, and repairs, potential failure of PT systems may lead to significant consequences.

Although there is a need for routine inspection of PT systems using nondestructive evaluation (NDE) techniques, it is not widely used by a majority of the bridge owners. A survey of the various US State Departments of Transportations [7,8] show that about half of the survey respondents did not use any NDE methods during their routine visual inspection, and only 10% of the respondents used NDE inspection techniques for routine in-depth inspections in a period spanning between 2 and 10 years. Among various other factors, the lack of knowledge and limitations of the existing NDE techniques for the condition assessment of PT systems are major roadblocks for their widespread use. As inspection and replacement of PT systems are expensive, guidelines are necessary to assist engineers in assessing the condition of these systems, and to correlate this information with the structural performance and provide recommendations to mitigate or prevent the deterioration process. In particular, reliable NDE techniques that can detect deterioration of the steel strands within PT systems are necessary. It is important to evaluate NDE technologies on control specimens to identify their advantages and shortcomings before adopting them for field inspection of steel strands in PT systems.

McGogney [9] summarized the Magnetic Field Disturbance method and the Magnetic Perturbation for Cables inspection system, two techniques that were available at that time, for the inspection of steel elements in concrete bridges. Although these methods showed good promise, disadvantages included difficulty in correlation analysis and the size and weight of the equipment. These drawbacks led to the development of the Magnetic Flux Leakage (MFL) system that could effectively detect loss in metallic area (LMA) in ferrous material, such as wire ropes used in mines and offshore cranes [10–15].

The principle of magnetic methods is to induce a magnetic field onto ferromagnetic materials such as steel cables/strands. When an external magnetic field of sufficient strength is applied near the ferrous material, all the atomic dipoles of the ferrous material align themselves with the external magnetic field, and is referred to as magnetic saturation [16]. When the external magnet is aligned along the longitudinal axis of the steel cable/strand, the flux lines will also be collinear with the longitudinal axis. Any reduction in the cross-sectional area of the steel cable/strand will cause the flux lines to move into the surrounding medium, typically referred to as flux "leakage". In the MFL technique, the flux leakage is measured using sensors, such as the Hall-effect sensor or coil sensor [11].

MFL methods can be classified into active MFL and residual MFL. In the active MFL method, a portable magnet is used to magnetize the ferrous material to induce magnetic flux at the saturation level between the two poles. At locations where there is a "leak" in the magnetic flux due to reduction in the cross-sectional area, sensors placed between the magnetic poles are used to measure this leakage in the magnetic flux. This gives an indication about the location of the flaws in the steel cables/strands. In the residual MFL technique, the specimen is first magnetized to saturation and then a device is used to measure the residual magnetic field, thereby detecting damages to the ferrous material. While active MFL is primarily useful for detecting large metallic defects, residual MFL is better at determining smaller defects [17].

The MFL technique has also been used for the evaluation of internal strands in bridge girders, parking decks, factories, indoor pools, and circumferential tendons of oil tanks [18–20], under both laboratory and field conditions. MFL showed good promise in detecting section loss in embedded strands in box girders and slabs with good accuracy [21]. However, the density of mild steel reinforcement around the tendons, the physical gap between the defects, and the degree of damage to be detected influenced the accuracy. Finite element simulations to investigate the influence of these parameters have also been conducted [22]. Superconducting quantum interference devices [23,24] used to

inspect prestressed tendons in deck slabs of a concrete highway bridge also showed good promise in detecting broken strands. Induced Magnetic Field (IMF) is a more recent development [25,26], which gives a direct measure of the undamaged volume of steel by measuring the induced magnetic field. However, this technique faces several challenges and has not yet been evaluated in the field.

MFL is a promising NDE technique for locating loss in metallic area of strands due to corrosion, pitting, or breakage, in external tendons of post-tensioned girders and the stay cables of cable-stayed bridges [17]. Several researchers [17,23,24,27–29] have developed MFL based devices consisting of magnets that magnetize the steel strands, and various configurations of sensors to detect leakage in the magnetic flux. Most devices performed well under controlled laboratory conditions in detecting defects in the steel strands, however they were either not verified or posed challenges under field conditions [27–29]. Several factors affected the performance of MFL under field conditions, which include the cross-sectional area and number of strands in the prestressing tendons, duct material, location of the sensor with respect to the defects, strength of the magnets, magnetic properties of steel, and the presence of cover concrete and other ferromagnetic components [28]. MFL inspection of stay cables also required extensive preparation of the cable surfaces in addition to safety considerations due to the strong electromagnetic field. The cost and self-weight of the equipment also pose challenges in the application of this technique [30]. In addition, application of MFL requires field calibrations using identical cables to determine the relationship between magnetic permeability and strain in the cables [31].

The loss in total strand cross-sectional area in an external PT system could vary anywhere between 0% and 100%, and it is important to identify severe cases of deterioration. Therefore, it was found appropriate to use an active MFL technique for the evaluation of the external PT tendons, as residual MFL is mainly applicable for detecting smaller areas of corrosion [17]. In the current investigation, a commercially available MFL device that has been successfully used for the detection of loss in metallic area in wire ropes is used to inspect strands embedded in HDPE (High Density Polypropylene) ducts filled with grout, under real-world field conditions. In addition, the limited clearance between the tendon to be inspected and the surrounding external tendons and/or the bottom slab of the girder, typically encountered in the field, pose severe limitations in wrapping the full-head of the sensor around the tendons. Therefore, the feasibility of using a half-head configuration of the MFL device to detect and quantify metal defects is also explored in this investigation.

The intent of this investigation is not to develop a new device for the inspection of strand defects. The major objectives of this investigation may be summarized as:

(a) Evaluate the capability of MFL in qualitatively and quantitatively measuring the loss in metallic area in external PT systems of a full-scale box girder under actual field conditions, using a commercially available device.

(b) Evaluate if the metal ducts in the anchorage region and deviators influence the identification of strand defects on external PT systems.

(c) Identify the capabilities and limitations of the MFL technique in detecting strand corrosion, section loss, and breakage in the external tendons of bridge PT systems in full-scale box girder under actual field conditions.

(d) Evaluate if half-head of the sensor can be used to identify metallic defects within external post-tensioning systems. This is especially useful when there is limited clearance around tendons to be evaluated and the surrounding tendons or the deck slab.

(e) Quantify the loss in metallic area based on the inspection results and compare them with the actual loss in metallic area.

This investigation is part of a larger experimental program, the

details of which may be found in Hurlebaus et al. [7,8]. While the evaluation of both grout and strand defects was part of the larger study, the evaluation of strand defects alone is presented in this paper.

2. Experimental program

The capability of active MFL in detecting corrosion, section loss, and breakage of strands in external tendons of in-service PT system under field conditions are investigated. To enable this evaluation, a full-scale post-tensioned girder specimen with known metal defects was fabricated. The defects were introduced into the mock-up specimen in a controlled manner. A brief discussion on the fabrication and placement of the strand defects, the fabrication of the girder specimen, a description of the equipment, inspection procedure and data interpretation, and the evaluation of the external tendons of the post-tensioned girder specimen using MFL are described in what follows. The evaluation of grout defects is presented elsewhere [32,33], and will not be discussed herein.

2.1. Fabrication of defects

To enable a comparison of the actual defects with the defects identified using the MFL technique, strand defects that are typically observed in external PT systems were fabricated, and the size and location of these defects in the girder specimen were documented. The defects included single-strand and multi-strand corrosion; wire, single-strand and multi-strand cross-section loss; and single-strand and multi-strand breakage. Table 1 presents a description of the metal defects, including their level of severity, and Fig. 1 presents representative images of the fabricated metal defects. The fabrication of each of the strand defects is discussed briefly in what follows.

2.1.1. Corrosion

The fabricated corrosion defects range from light strand pitting to complete strand corrosion. Fig. 1(a) shows the general electrolytic corrosion cell, consisting of an electrical power source, an acid bath, and electrodes, that was used to achieve corroded strand conditions. The acid bath was a mix of water, hydrochloric acid, and sodium chloride. To induce corrosion in the strand, electric current was passed through the electrode and the strands were immersed in the acid bath. However, this process of fabricating the corroded strands to achieve the desired reduction in cross-sectional area required that the strands be immersed in

the acid bath for a significant period of time. Considering time limitations, the required reduction in cross-sectional area was achieved by mechanically grinding the strands over a length of about 610 mm to the desired reduced cross-sectional area using a grinding wheel. The strands with the reduced cross-sectional area were then immersed in the electrolytic corrosion cell for a period of 48 hours until by-products of residual corrosion were formed (Fig. 1b and c). To simulate severe strand corrosion, all the wires of the strands were cut at the desired location and immersed in the electrolytic corrosion cell (Fig. 1c). A combination of individual strands with complete loss in cross-sectional area was used to obtain defects with the desired loss in overall strand cross-sectional area.

This method helped to accelerate the fabrication of the corrosion defects, and at the same time ensured that an ample amount of corrosion by-products formed around the strands to simulate corrosion defects. Although, this procedure may not lead to formation of mild to severe pitting found in real corrosion conditions, the primary aim was to create sufficient corrosion by-products.

2.1.2. Section loss

Loss in cross-sectional area of the strands may occur due to fatigue, inter- and intra- strand wear, in addition to corrosion [34]. Fig. 1(d)–(h) shows representative images of section loss that were fabricated in the wires and strands. Also presented in the figure is the range of the final diameters to which the strands were mechanically ground, to obtain the desired loss in metallic area. Fig. 1(h) shows the most severe strand section loss (LS3), where there is discontinuity in all seven wires of the strand.
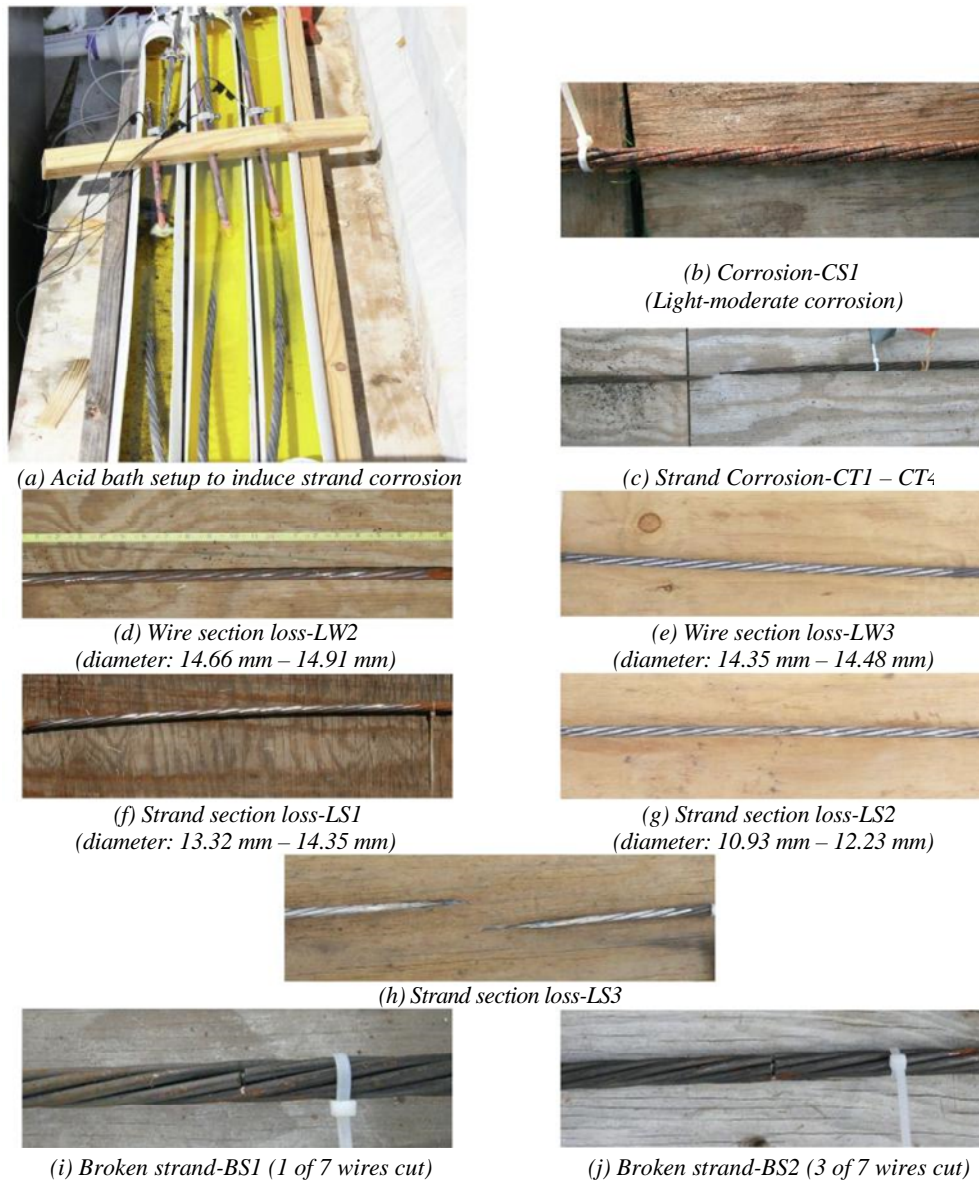
2.1.3. Breakage

Breakage of strands and tendons typically occurs due to excessive fatigue loads on the PT systems [35,36]. They could also occur due to overstressing of the PT strands, especially in the presence of pre-existing pitting. Single-strand and multi-strand breakage conditions were fabricated by making vertical cuts across the strands. Fig. 1(i)–(j) shows typical strand breakages that were fabricated. Depending on the severity of the breakage, 1–3 wires of the strand were cut using a cutting wheel.

2.2. Placement of defects

To validate the effectiveness of the MFL technique in detecting metal defects in external PT systems, the location of the defects along the length of the tendon were documented accurately. The external

Table 1
Description of metal defects in the external post-tensioning tendons.

	Condition type	Defect code	Condition description
Section Loss	Wire	LW1	< 15% (light) loss in wire cross-sectional area (< 1% TSCS)
	Section loss	LW2	35–65% (severe) loss in wire cross-sectional area (< 1% TSCS)
		LW3	Extreme loss in wire cross-sectional area (< 2% TSCS)
	Single-strand section loss	LS1	1–2 of 7 wires fully lost (< 3% TSCS)
		LS2	3–4 of 7 wires fully lost (2–5% TSCS)
		LS3	7 of 7 wires fully lost (5–9% TSCS)
	Multi-strand	LT1	1–2 of 19 strands fully lost (5–16% TSCS)
	Section loss	LT2	3–4 of 19 strands fully lost (16–25% TSCS)
		LT3	9–10 of 19 strands fully lost (47–59% TSCS)
		LT4	19 of 19 strands fully lost (100% TSCS)
Corrosion	Single-strand corrosion	CS1	1–2 of 7 wires fully corroded (< 3% TSCS)
	Multi-strand corrosion	CT1	1–2 of 19 strands fully corroded (5–16% TSCS)
		CT2	3–4 of 19 strands fully corroded (16–25% TSCS)
		CT4	19 of 19 strands fractured (100% TSCS)
Breakage	Single-strand breakage	BS1	1 of 7 wires fractured (< 2% TSCS)
		BS2	3 of 7 wires fractured (2–4% TSCS)
	Multi-strand breakage	BT1	1 of 19 strands fractured (5–8% TSCS)
		BT2	3 of 19 strands fractured (16–17% TSCS)
		BT3	10 of 19 strands fractured (50–53% TSCS)
		BT4	19 of 19 strands fractured (100% TSCS)
Undamaged strand(s)		NMD	No metallic defects

TSCS = Total Strand Cross-Section for the group of strands in the tendon

(a) Acid bath setup to induce strand corrosion

(b) Corrosion-CS1
(Light-moderate corrosion)

(c) Strand Corrosion-CT1 – CT4

(d) Wire section loss-LW2
(diameter: 14.66 mm – 14.91 mm)

(e) Wire section loss-LW3
(diameter: 14.35 mm – 14.48 mm)

(f) Strand section loss-LS1
(diameter: 13.32 mm – 14.35 mm)

(g) Strand section loss-LS2
(diameter: 10.93 mm – 12.23 mm)

(h) Strand section loss-LS3

(i) Broken strand-BS1 (1 of 7 wires cut)

(j) Broken strand-BS2 (3 of 7 wires cut)

Fig. 1. Representative images of the fabricated strand defects.

post-tensioning HDPE ducts were divided into 914 mm (3 ft) long segments, and it was ensured that all the metal strand defects were placed close to the center of these segments. The defective strands were distributed across the cross-section of the tendon, as would be the case in a typical PT tendon. Typically, strand segments belonging to three complete strands were placed at a time. Following the placement of the strand segments, a polyurethane non-sag sealant was placed through the openings in the external ducts on either side of the 914 mm long duct segment. The sealant ensured that the strand segments did not move during the placement of additional strands or during the test. The impervious layer of the sealant was gradually built-up on either side of the 914 mm long duct segment for the placement of grout. The grouting operation was performed using a grout pump from the anchorage regions or through the access holes in the HDPE ducts. After the grout hardened, the access holes were sealed off with HDPE caps to prevent the infiltration of moisture.

### 2.3. Description of the post-tensioned girder specimen

A full scale post-tensioned U-beam girder specimen with both internal and external tendons was constructed to serve as the control specimen. The girder specimen was constructed at the Texas A&M University RELLIS Campus in Bryan, Texas. Fig. 2 shows the details of the girder specimen which is 22.86 m long, 4.19 m wide, and has an overall height of 1.85 m from the bottom of the slab to the top of the flange. Of the 20 tendons shown in section D-D in Fig. 2, tendons T15-T20 are external tendons with a harped profile. Smooth HDPE ducts with an outer diameter of 114 mm, and a wall thickness of 2.5 mm were used for the external tendons. However, steel pipes were used within the anchorage regions and the deviators of the girder specimen. Each external tendon had a total of 19 seven-wire 15.2 mm diameter strands. To ensure that the external tendons were taut resulting in minimum deflection and sagging of the tendons during inspection, one continuous strand of each of the six external tendons was stressed to a prestressing force of 13.3 kN (3 kips).

2.4. Description of the equipment

Fig. 3 shows the schematic and photographs of the LMA-450 sensor head along with the CC-04 USB signal console manufactured by NDT Technologies Inc. that was used for the inspection of the external tendons. The LMA-450 sensor head is capable of testing external tendons
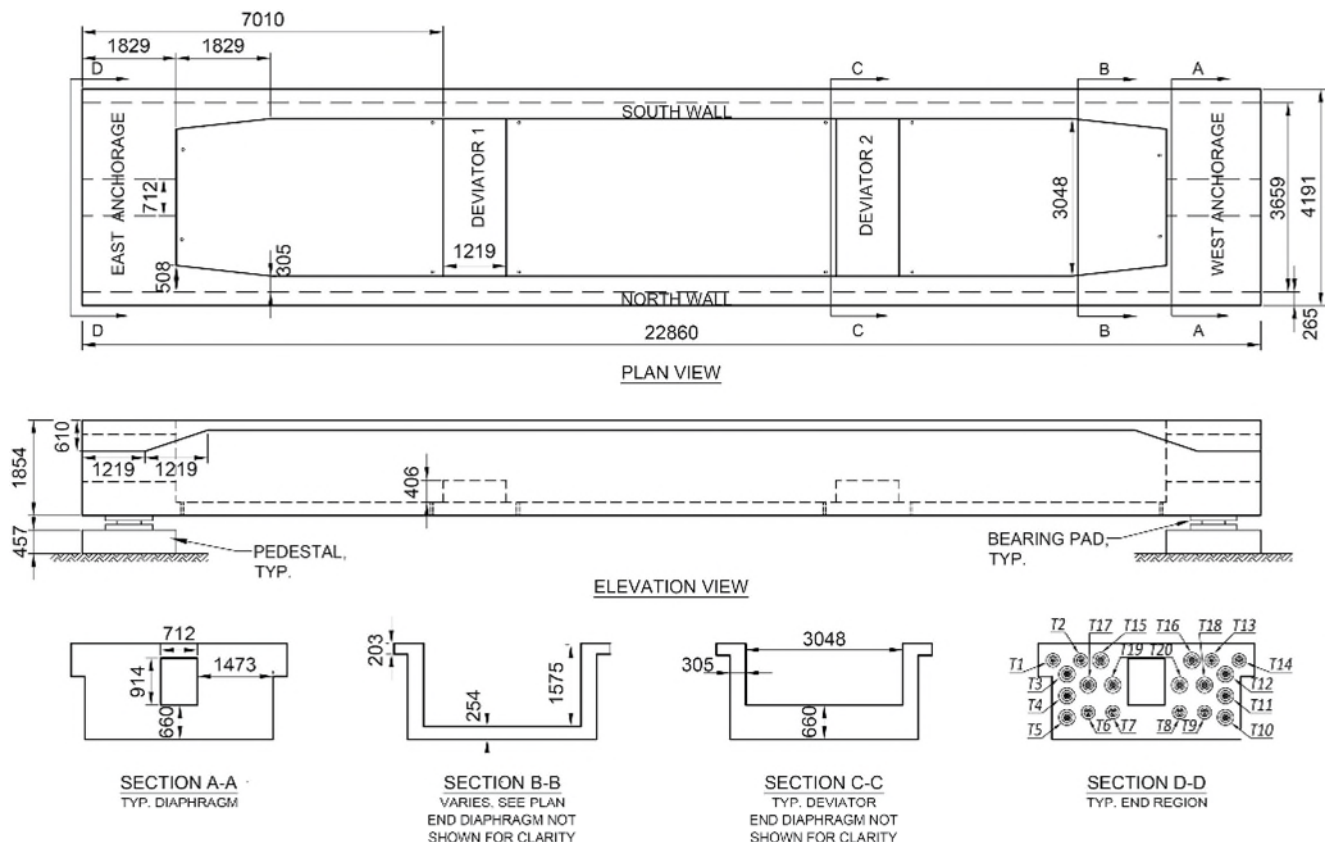
Fig. 2. Layout and cross-sectional details of post-tensioned U-beam girder specimen.

up to 120 mm diameter. The sensor head is usually used for the inspection of wire ropes, and is capable of detecting loss in metallic area caused by external and internal corrosion, wear, or change in wire rope structure; and localized flaws caused by broken wires and corrosion pitting. The sensor head shown in Fig. 3(b), (c) consists of a strong permanent magnet assembly, a sensor assembly, and a distance counter wheel assembly. The device consists of a set of permanent magnets, one on each side of the tendon to be inspected which are connected using ferro magnetic bars. This provides a return path for the magnetic flux between the magnets. In this setup, the magnets form the pole pieces to generate the flux in the tendon at a saturation level. Sensing coils are in a plane transverse to the magnetic poles, with one end located in close proximity to the exterior surface of the cable for detecting perturbations in flux caused by defects. Another portion of the coil extends around the outside and circumscribes the return flux path through the ferro magnetic bar. This configuration allows for easy mounting and demounting of the equipment on cables at any intermediate section. Further details of the equipment and the circuitry can be found in Weischedel [11].

The strong permanent magnets in the sensor head are directly used on the external post-tensioning system to magnetize the ferrous material (steel). This induces flux paths in the material between the two poles of the magnet. In regions where there is loss in cross-sectional area of the metal strands, the magnetic field in the material "leaks" from its typical path. A magnetic field detector comprised of coils between the poles of the magnet is sensitive to this change in magnetic field and indicates the leak. A signal console shown in Fig. 3(d) is used to gather data from the sensor head. The signal console consists of a signal conditioning circuitry, integrated chart recorder, an USB port for interface with a computer, and interface circuitry and connectors for both an external chart recorder and an external data acquisition system. The USB port connection may be used to display and store data in a computer.

The full-head and half-head sensor configurations shown in Fig. 3(b) and (c) respectively, may be used for the inspection of the external PT tendons. While the full-head configuration is usually preferred, under actual field conditions it may be difficult or even impossible to wrap the sensor heads around the PT duct due to limited clearance between the external tendons and/or the bottom slab of the girder. In order to address this accessibility issue, in this study, only the half-head sensor is used for the evaluation of the external tendons.

2.5. Inspection procedure and data interpretation

The advantage of using MFL for the inspection of external PT systems is that it does not need any extensive site preparation. However, it is recommended to ensure that the surface of all the external tendons to be inspected are clean and free of debris. It is also recommended to have an appropriate marking system to identify the tendon and the location of the defects along the length of the tendon. The equipment should be calibrated and validated on-site against any ground truth data that might be available at the inspection location. However, in the absence of ground truth data, a mock specimen with known strand properties should be used to calibrate and validate the accuracy of the device for detecting specific strand conditions. In the present study, an external calibration strip made of thin metallic wires, whose total area was 1% of the total cross-sectional area of the group of strands in the tendon in the duct was used.

The MFL device used in this study recorded both the LMA and Localized Flaw (LF) traces. The LMA trace gives a quantitative measure of most of the loss of cross-sectional area of the strand. However, the LF trace indicates only extremely localized flaws that are typically caused by broken wires and corrosion pitting. In addition, the LF trace show peaks at the beginning and end of elongated defects. Owing to this, the interpretation of defects associated with the LF trace is cumbersome. In
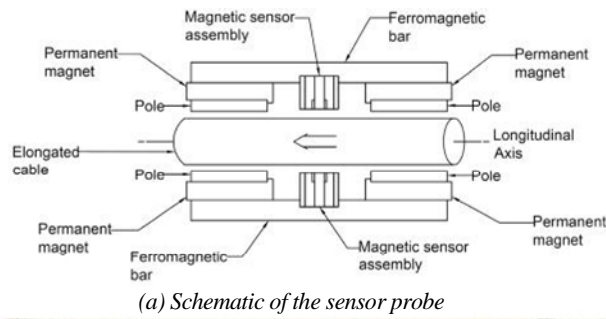
(a) Schematic of the sensor probe

(b) Full-head sensor

(c) Half-head sensor

(d) USB signal console connected to laptop

Fig. 3. Experimental setup, and components of MFL inspection technique.

addition, the LF trace provides only a qualitative measure and cannot be calibrated, thereby being of limited value to assess the extent of deterioration. Due to these reasons, the LF trace is not considered further in this study. After the data was acquired and input into the data analysis software (NDT_CARE™), LMA enhancement and post-calibration of the data was performed. The calibration was performed by
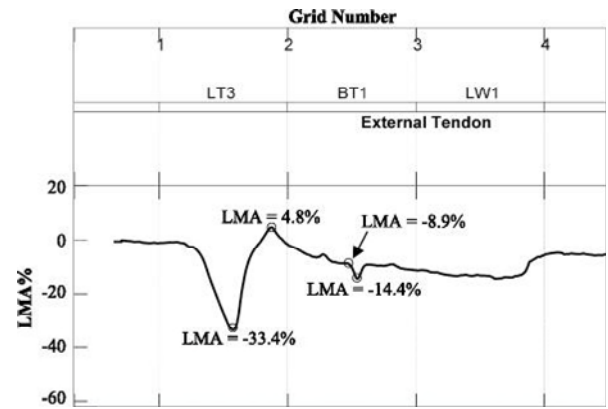
Fig. 4. Validation of data from MFL device with known defects.

adjusting the peak in the LMA signal caused by the known calibration strip to the appropriate increase in cross-sectional area. The rest of the peaks in the inspection data scaled according to the calibration data. To quantify the loss in tendon cross-sectional area, the difference in LMA percentages between the valley and peak observed in the record data are considered. For example, in Fig. 4, the loss in tendon cross-sectional area corresponding to the spike observed at the location of defect LT3 may be quantified as 38.2%, which is the absolute difference between the LMA percentages of –33.4% and 4.8% observed at the peak and valley respectively.

2.6. Validation of the half-head sensor

The aim of the study is to assess the capability of the MFL technique to detect strand defects in in-service bridges exposed to environmental conditions. To ensure the accuracy and reliability of the inspection results, the device was validated against known defects on a control specimen under similar field conditions. A straight external HDPE tendon, with epoxy coated strands and no protective grout in the duct, was used to validate the accuracy of the results. Strand defects with known loss in cross-sectional area were fabricated and placed at pre-determined locations within the HDPE ducts of the control specimen. Fig. 4 shows a comparison of the location of the actual defects with the results obtained using the half-head of the sensor. While the half-head configuration is unable to identify very small loss in cross-sectional area (< 1% of the total strand cross-section), larger defects are positively identified with distinct spikes in the acquired data. From Fig. 4, the LMA for defects LT3 and BT1 may be quantified to be approximately 38.2% and 5.5%, respectively, which is close to the actual LMA of 47–59% and 5–8%. In addition, there are no false positives that were indicated during the inspection. This clearly shows that the half-head configuration of the sensor shown in Fig. 3c can be used not only to identify the metal defects, but also to quantify the defects with reasonable accuracy.

2.7. Evaluation of external post-tensioning system using MFL

All six external tendons T15-T20 of the U-girder were inspected using the half-head of the MFL device. For each of the tendons, the sensor head was moved forward and backward along the length of the external duct. Four trials per external tendon were carried out, resulting in a total of eight measurements per external tendon. The multiple readings were used to assess the repeatability of the measurements.

The distance between the face of the anchorage regions/deviators and the center of the sensor head was greater than 610 mm for all segments of the external tendons. Therefore, LMA percentage measurements could not be made in the sections of the tendons next to the anchorage regions and deviators.
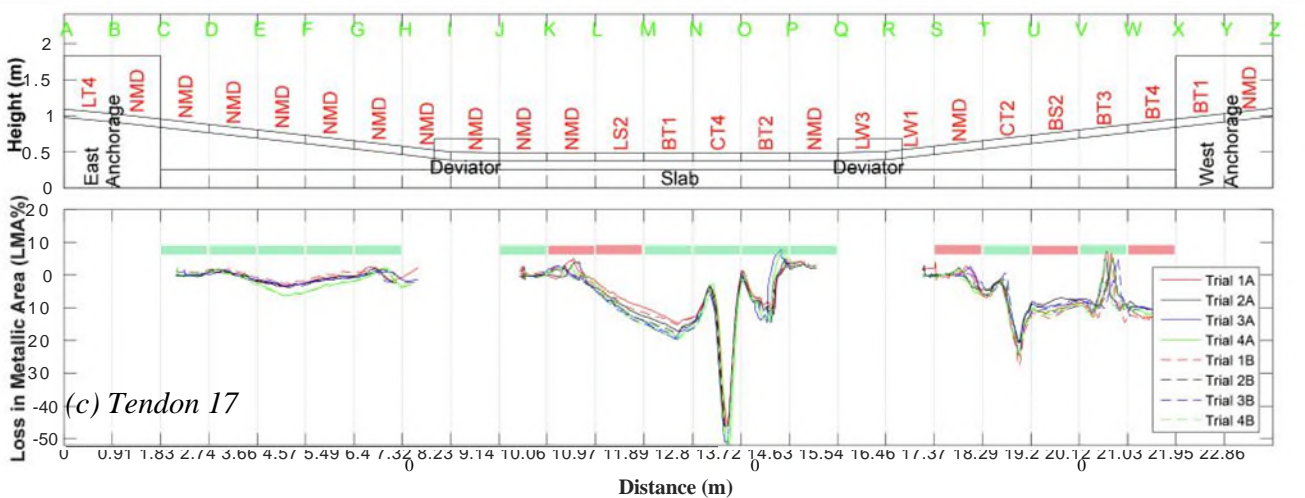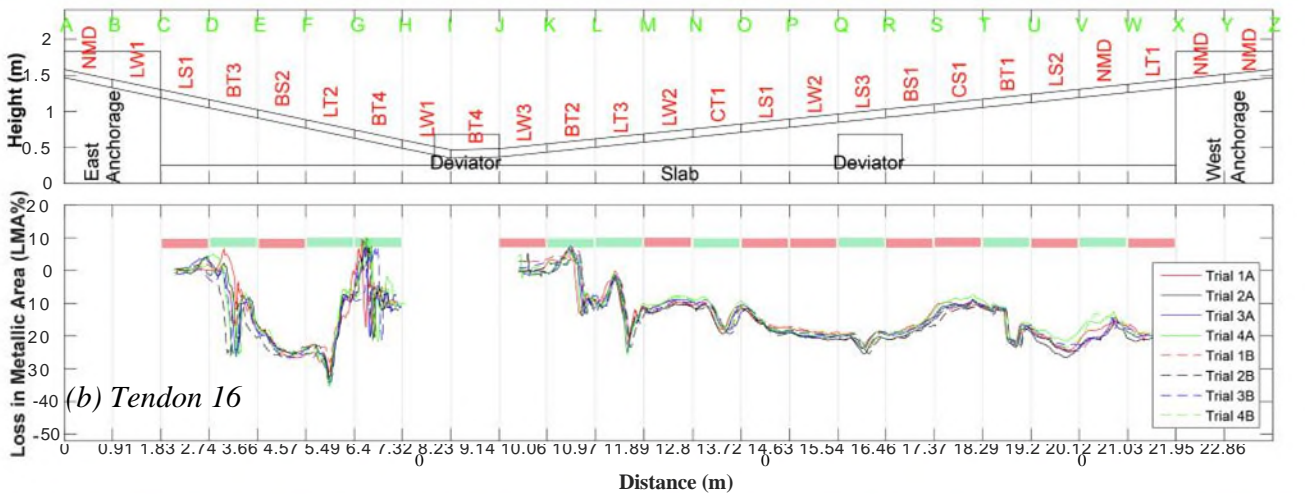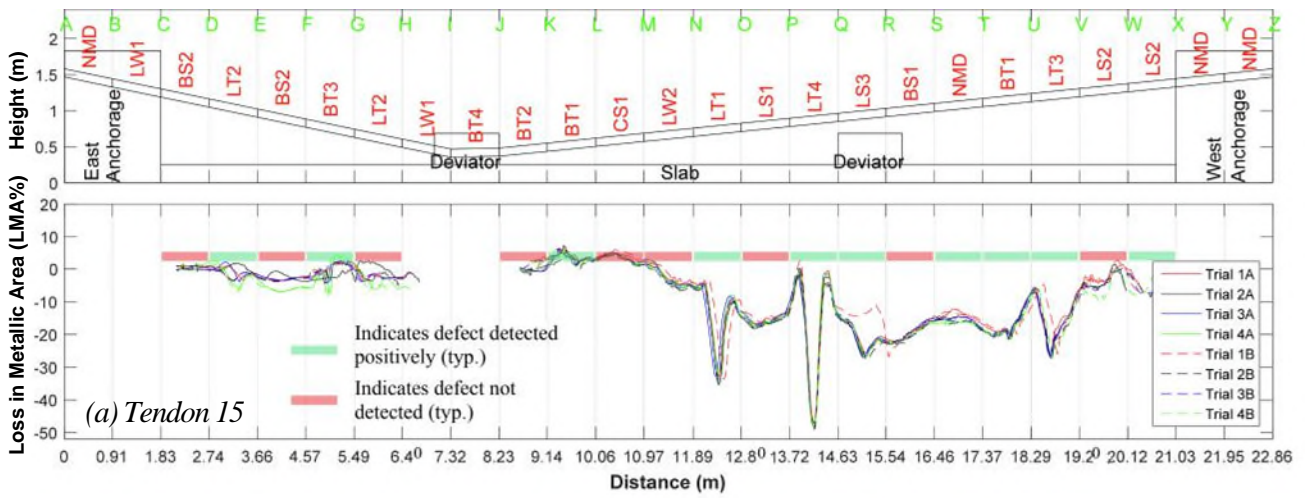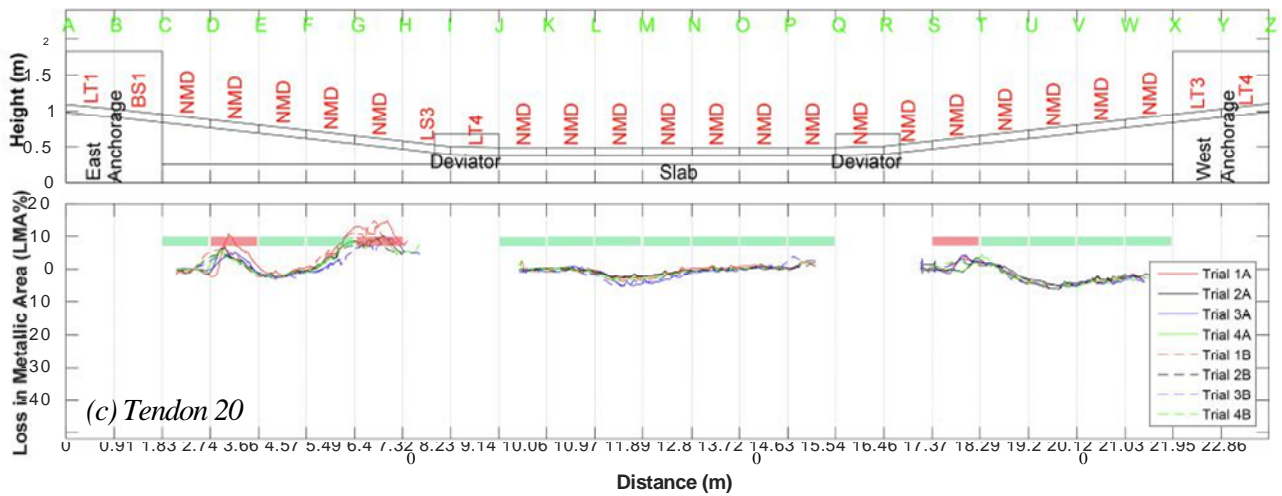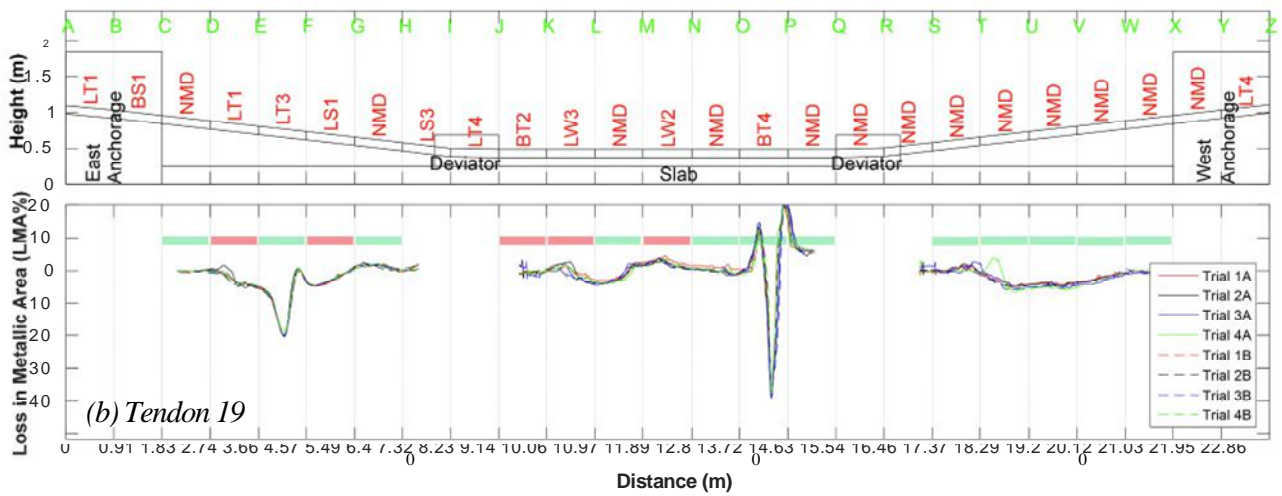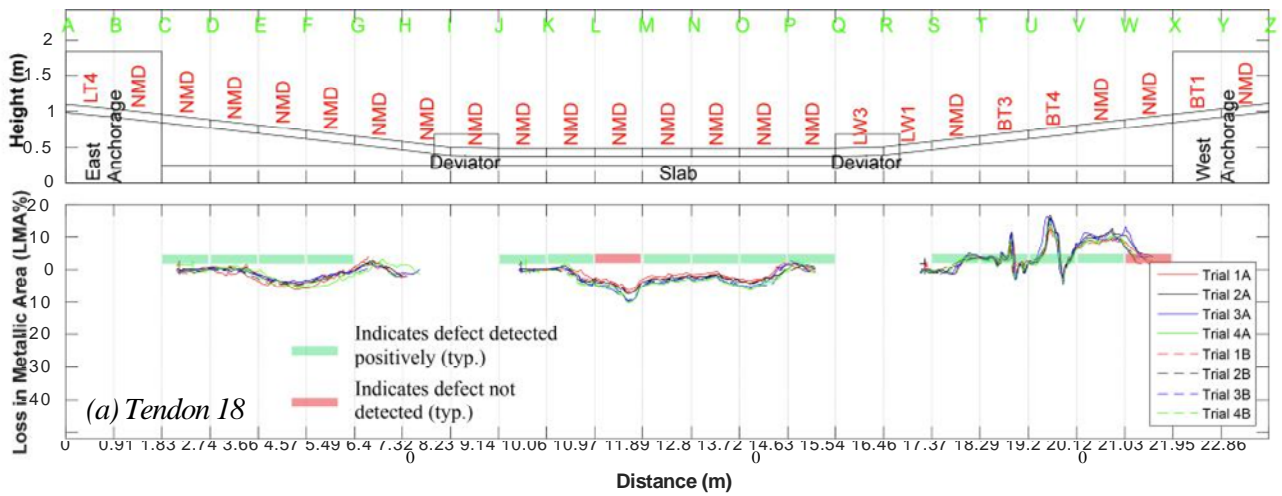
Note: Typical distance between grid points = 914 mm (3 ft). Defect description may be found in Table 1.

Fig. 5. Comparison of results from MFL using half-head sensor with the actual defects-External Tendons 15, 16, and 17.

3. Inspection results

Figs. 5 and 6 present a comparison of actual defects with the results from the inspection of external tendons of the post-tensioned girder using half-head of the MFL device. The inspection results are evaluated for accuracy in detecting the location of the defect, and the severity of the defect. It is to be noted that the LMA percentages for the sections of the tendons without any strand defects do not follow the zero LMA percentage line. This pattern is attributed to the magnetic offset levels, and the end effects. The magnetic offset is attributed to the change in volume of the ferromagnetic material that the magnets are exposed to at the time of test when compared to its previous state. On the other

(a) Tendon 18

(b) Tendon 19

(c) Tendon 20

Note: Typical distance between grid points = 914 mm (3 ft). Defect description may be found in Table 1.

Fig. 6. Comparison of results from MFL using half-head sensor with the actual defects-External Tendon 18, 19, and 20.

hand, the end effect which is a low frequency component in the output signal, is a local phenomenon that arises due to the distortion of the magnetic field at the ends of the external tendons, and due to the re-magnetization effect. The remagnetization effect causes variation in the permanent magnetization of the strands in the tendons as the sensor head moves along the tendon. However, despite these patterns and as described earlier, the loss in metallic area may be identified by a sudden

peak (or valley) that are observed in the recorded data.

Fig. 5(a) presents results from all eight trials for external Tendon 15. Due to the presence of the deviator, external Tendon 15 was inspected in two sections, between section C-I and section J-X. However, due to lack of accessibility, the sections close to the deviator (H-I, J-K) could not be inspected. Single-strand breakage BS1 in section R-S and BS2 in section E-F were not positively identified. Single-strand corrosion CS1

in section L-M was also not identified from the inspection results. Similarly, wire section loss LW2 in section M-N, and single-strand section loss LS1 in section O-P were not evident from the inspection results. However, one of the two single-strand section loss LS2 between section V-X could be vaguely identified. All these defects that could not be identified using MFL had a loss in total strand cross-sectional area of less than 5%.

Single-strand section loss LS3 in section Q-R was evident from the distinct peak. Multi-strand section loss LT1 in section N-O, LT3 in section U-V, and LT4 in section P-Q, could all be easily identified from the distinct peaks observed from the inspection results. Multi-strand section loss LT2 in sections D-E is vaguely discernable, however LT2 in section G-H is not identified between the various trials. Multi-strand breakage BT1 in sections K-L, and T-U; and BT3 in section F-G could be identified from the small peaks observed from the inspection data.

Similar results with a few exceptions are observed from the inspection results of the remaining external tendons. Owing to the large number of defects in the external tendons, the results are not discussed individually, but are shown in Figs. 5 and 6.

The raw data obtained from the inspection were extremely consistent within the various trials, demonstrating the repeatability of the method. While processing the raw data from the inspection is relatively straight forward, there could be some concerns while calibrating the data with respect to the calibration strip. The calibration strip, which had a cross-sectional area of 1% of the total cross-section of all the strands in the tendon, may be appropriate to scale defects with small loss in cross-sectional area, such as CS1. However, this may not be appropriate to scale larger loss in metallic area, such as CT4/LT4. This could likely lead to some discrepancies in quantitatively estimating the loss in metallic area. It was observed that the relative percent to which the data were calibrated had to be consistent among the various trials, to obtain comparable final outcomes.

Figs. 5(c) and 6(a) show a positive LMA percent in section V-W of Tendon 17 and section U-V of Tendon 18, indicating an apparent increase in metallic area. This observation is consistently made between the various trials. It is to be noted that in between sections V-X in Tendon 17 and T-V in Tendon 18, there were multiple 914 mm long strand sections that simulate a broken tendon. During the placement of the strands in these sections, it is likely that the smaller 914 mm long strand sections could have slightly displaced from their intended location before the placement of the sealant. This could be the possible reason for the net increase in metallic cross-sectional area in the adjacent region.

4. Discussion

Table 2 presents a summary of the total number of defects that were inspected, and that were positively identified by the MFL inspection technique. Also presented in Table 2 are the overall percentage of defects that were detected. Considering defects with less than 5% loss in tendon cross-sectional area, only one of the total 22 defects was identified positively, leading to a detection rate of under 5%. However, 25 out of the total 31 defects with a loss in cross-sectional area greater than 5% were positively identified, resulting in a detection rate of about 80%. The defects that could be identified included the multi-strand breakage (BT1-BT4), multi-strand corrosion (CT1-CT4), loss in multi-strand cross-sectional area (LT1-LT4), and high loss in single-strand cross-sectional area (LS3). However, single-strand corrosion (CS1), loss in wire cross-sectional area (LW2-LW3) and single-strand cross-sectional area (LS1-LS2), and single-strand breakage (BS1-BS2), all with under 5% loss in total strand cross-section, have a very low probability of being detected on a consistent basis. Therefore, in general, it may be stated that loss of total strand cross-sectional area greater than 5% could be identified relatively easily and with high probability of detection.

Table 3 presents a comparison of the average LMA of the fabricated defects with the average estimated LMA obtained from inspection using

Table 2
Summary of results for identifying location of strand defects.

Condition type	Defect code	Total No. of Defects	Identified	% Detected
		positively inspected		
Wire	LW2	4	0	0
section loss	LW3	2	0	0
Single-strand	LS1	4	0	0
section loss	LS2	4	1	25
	LS3	2	2	100
Multi-strand	LT1	3	1	33
section loss	LT2	3	2	67
	LT3	3	3	100
	LT4	1	1	100
Single-strand corrosion	CS1	2	0	0
Multi-strand corrosion	CT1	1	1	100
	CT2	1	1	100
	CT4	1	1	100
Single-strand breakage	BS1	2	0	0
	BS2	4	0	0
Multi-strand breakage	BT1	4	4	100
	BT2	4	2	50
	BT3	4	4	100
	BT4	4	3	75
Undamaged strand(s)*	NMD*	52	45	87

* False positives.

the MFL technique. The difference between the LMA percentages at the apex and the valley of the peaks in the signal, as described earlier, were used to arrive at the estimated LMA percent. As there were a total of eight trials, the average of all the trials was considered as the final estimated LMA percent. Table 3 also presents the error between the actual and estimated LMA percentages. In general, the average error increases as the loss in metallic area increases. For defects where the actual average loss in metallic area was less than 21%, the error between the actual LMA and measured LMA was in the range of

Table 3
Comparison of severity of actual defects with results from MFL for external post-tensioning tendons.

Defect code	Tendon (T) #	Section	Actual average loss in metallic area (%) [A]	Estimated average loss (%) in metallic area (%) [B]	Error |A B|	Average error (%)
CT1	T16	N-O	10.5	8.2	2.3	2.3
CT2	T17	T-U	20.5	17.9	2.6	2.6
CT4	T17	N-O	100.0	46.9	53.1	53.1
LS2	T15	W-X	3.5	4.1	0.6	0.6
LS3	T15	Q-R	7.0	8.6	1.6	1.8
	T16	Q-R		4.9	2.1	
LT1	T15	N-O	10.5	27.1	16.6	16.6
LT2	T15	D-E	20.5	3.8	16.7	13.4
	T16	F-G		10.4	10.1	
LT3	T15	U-V	53.0	19.8	33.2	35.4
	T16	L-M		15.7	37.3	
	T19	E-F		17.2	35.8	
LT4	T15	P-Q	100.0	45.9	54.1	54.1
BT1	T15	K-L	6.5	2.0	4.5	3.4
	T15	T-U		3.5	3.0	
	T16	T-U		8.3	1.8	
	T17	M-N		2.0	4.5	
BT2	T16	K-L	16.5	10.3	6.2	6.0
	T17	O-P		10.6	5.9	
BT3	T15	F-G	51.5	6.0	45.5	38.8
	T16	D-E		18.7	32.8	
	T17	V-W		16.9	34.6	
	T18	T-U		9.3	42.2	
BT4	T16	G-H	100.0	21.4	78.6	78.6

0.60–17%. However, when the actual average LMA was greater than 50%, such as in the case of CT4, LT3, LT4, BT3 and BT4, the associated error in the measured LMA were in the range of 35–79%. Most of these measured values were less than the actual LMA percentages. This is likely because, despite best efforts during the placement of defects, the strand defects were possibly not aligned in one vertical plane of the cross section of the tendon, thereby resulting in an underprediction of the LMA percentage. Additionally, as noted in earlier studies, the small separation between the defects could also have an impact on the measured LMA percentages. Even though, there are errors associated with the estimated LMA percentages, the estimated magnitude of the loss in total strand cross-sectional area gives a good indication about the severity of the defect that may be expected at that location.

5. Conclusions

The capability of the Magnetic Flux Leakage method in detecting loss in metallic area in external post-tensioning systems of in-service bridges was assessed in this investigation. The results are generally positive in terms of the potential for the MFL method in locating and estimating the loss in metallic area within external post-tensioning systems. The following specific conclusions were drawn from this study.

1. The MFL method is efficient in detecting strand defects in the free spans of external tendons under actual field conditions.
2. In regions where there is limited clearance around external tendons, a half-head sensor of the permanent magnet can be effectively used for inspection. However, a comparative experimental study is required between a half- and a full-head sensor, to investigate the limitations of the half-head sensor in terms of detecting defects with less than 5% LMA, and in quantifying the severity of defects.
3. The raw data gathered from the MFL inspection clearly indicated that the inspection technique is highly repeatable and reproducible. About 80% of the defects with a loss in tendon cross-sectional area greater than 5% was consistently identified by the MFL technique.
4. The MFL inspection adopted in this investigation was not very efficient in detecting metallic flaws when the LMA was less than 5% of the total strand cross-sectional area for the group of strands in the tendon. However, a majority of the defects with LMA greater than 5% were positively identified.
5. Although the MFL inspection technique used in this investigation is capable of detecting loss in metallic area caused by corrosion, section loss, or breakage; it cannot differentiate between these defects.
6. The majority of the MFL inspection data did not show any false-positive indications of strand defects.
7. The magnetic offset levels and end effects can make the interpretation of the results challenging. Owing to these effects, the output signals from the MFL inspection did not always indicate zero loss in metallic area in regions without any defects. Further investigations are necessary to determine if the use of the full-head of the permanent magnet, or the use of an annular coil will help overcome these shortcomings.
8. The metallic defects could typically be identified by a sudden change in slope in the recorded data.
9. Even though the MFL inspection technique employed in this study can locate loss in metallic area quite accurately, the estimated magnitude of the defect may not be relied upon completely. In general, the difference between the actual and measured values increased as the LMA increased. A majority of the estimated LMA were less than the actual LMA. Nevertheless, the estimated magnitude provides a good indication of the severity of the loss in metallic area.

Acknowledgements

Appendix A. Supplementary material

Supplementary data to this article can be found online at https://doi.org/10.1016/j.engstruct.2019.109765.

References

[1] Standing Committee on Structural Safety. Seventh Report of the Committee for the Two Years Ending in July 1987. EA/88/4; 1987.

[2] FDOT. Corrosion Evaluation of Post-Tensioned Tendons on the Niles Channel Bridge. Florida Department of Transportation, Tallahassee, Florida; 1999.

[3] Powers R, Sagüés A, Virmani Y. Technical Memorandum of Public Works Research Institute; 2002. p. 579–94.

[4] Corven Engineering. Mid bay bridge post-tensioning evaluation. Florida Department of Transportation, Tallahassee, Florida; 2001.

[5] FDOT. Sunshine skyway bridge post-tensioned tendons investigation. Florida Department of Transportation, Tallahassee, Florida; 2001.

[6] Hansen B. Tendon failure raises questions about grout in posttensioned bridges. Civ Eng 2007;77(11):17–8.

[7] Hurlebaus S, Hueste MBD, Karthik MM, Terzioglu T. Condition assessment of bridge post-tensioning and stay cable systems using NDE methods. NCHRP Project 14-28. Transportation Research Board, Washington, DC; 2017a.

[8] Hurlebaus S, Hueste MBD, Karthik MM, Terzioglu T. Inspection guidelines for bridge post-tensioning and stay cable systems using NDE methods. NCHRP Report 848. Transportation Research Board, Washington, DC; 2017b.

[9] McGogney CH. Magnetic flux leakage for bridge inspection. In: Nondestructive Testing Methods for Civil Infrastructure, Irvine, California, United States; 1993.

[10] Weischedel HR. The inspection of wire ropes in service: a critical review. Mater Eval 1985;43(13):1592–605.

[11] Weischedel HR. Method and apparatus for magnetically inspecting elongated objects for structural defects. Patent US Patent No. 4659991; 1987.

[12] Weischedel HR, Hoehle HW. Quantitative nondestructive in-service evaluation of stay cables of cable-stayed bridges: methods and practical experience. In: Proc. Nondestructive Evaluation of Aging Bridges and Highways, Oakland, California; 1995.

[13] Dohm M. An evaluation of international and local magnetic rope testing instrument defect detection capabilities and resolution, particularly in respect to low rotation, multilayer rope constructions. Project No. GAP 503 and GAP 353, Safety in Mines Research Advisory Committee, Johannesburg, South Africa; 1999.

[14] Smith DT, McCann P. Evaluation of instruments for the non-destructive testing of wire ropes. Report No. Fe/02/07. Health and Safety Laboratory, Sheffield, UK; 2002.

[15] Snyder MP. Non Destructive Safety Evaluation of a Hoist Rope PAR 101801. ID No. 36-08893. US Department of Labor Mine Safety and Health Administration, Triadelphia, West Virginia; 2012.

[16] Ghorbanpoor A. Magnetic-based NDE of steel in prestressed and post-tensioned concrete bridges. Struct Mater Technol 1998:343–9.

[17] Azizinamini A, Gull J. Improved inspection techniques for steel prestressing/post-tensioning strand: Volume 1. BDK80 977-13, Florida Department of Transportation, Florida International University; 2012.

[18] Scheel H, Hillemeier B. Location of prestressing steel fractures in concrete. ASCE J Mater Civil Eng 2003;15(3):228–34.

[19] Azizinamini A. Non-Destructive Testing (NDT) of a segmental concrete bridge scheduled for demolition, with a focus on condition assessment and corrosion detection of internal tendons. BDV29-977-05. BDV29-977-05, Florida Department of Transportation, Florida; 2017.

[20] Fernandes B, Titus M, Nims DK, Ghorbanpoor A, Devabhaktuni V. Field test of magnetic methods for corrosion detection in prestressing strands in adjacent box-beam bridges. J Bridge Eng 2012;17(6):984–8.

[21] Jones L, Pessiki S, Naito C, Hodgson I. Inspection methods and techniques to determine non visible corrosion of prestressing strands in concrete bridge components: Task 2 – assessment of candidate NDT methods. Pennsylvania Department of Transportation, Pennsylvania; 2010.

[22] Shams S, Al Ghorbanpoor, Lin S, Azari H. Nondestructive testing of steel corrosion in prestressed concrete structures using the magnetic flux leakage system. Transportation Research Board; 2018. p. 1–13.

[23] Krause HJ, Wolf W, Glaas W, Zimmermann E, Faley MI, Sawade G, et al. SQUID

system for magnetic inspection of prestressed tendons on concrete bridges. Insight Nondestructive Testing Cond Monit 2001;43(7):458–61.

[24] Krause HJ, Wolf W, Glass W, Zimmermann E, Faley MI, Sawade G, et al. SQUID array for magnetic inspection of prestressed concrete bridges. Physica C 2002;368(1):91–5.

[25] Fernandes B, Wade JD, Nims DK, Devabhaktuni VK. A new magnetic sensor concept for nondestructive evaluation of deteriorated prestressing strand. Res Nondestr Eval 2012;23(1):46–68.

[26] Nims D, Devabhaktuni V. Magnetic sensor for NDE of deteriorated prestressing strand-phase 1. The University of Toledo University Transportation Center, Toledo, Ohio; 2011.

[27] Ghorbanpoor A, Borchelt R, Edwards M, Abdel Salam E. Magnetic-based NDE of prestressed and post-tensioned concrete members-the MFL system. University of Wisconsin-Milwaukee; 2000.

[28] DaSilva M, Javidi S, Yakel A, Azizinamini A. Nondestructive method to detect corrosion of steel elements in concrete. P597. National Bridge Research Organization, Lincoln, Nebraska; 2009.

[29] Xu F, Wang X, Wu H. Inspection method of cable-stayed bridge using magnetic flux leakage detection: principle, sensor design, and signal processing. J Mech Sci

Technol 2012;26(3):661–9.

[24] Mehrabi AB. In-service evaluation of cable-stayed bridges, overview of available methods, and findings. J Bridge Eng 2006;11(6):716–24.

[25] Nazarian E, Ansari F, Zhang X, Taylor T. Detection of tension loss in cables of cable stayed bridges by distributed monitoring of bridge deck strains. J Struct Eng 2016;142(6):04016018.

[26] Terzioglu T, Karthik MM, Hurlebaus S, Hueste MBD. Nondestructive evaluation of external post-tensioning systems to detect grout defects. J Struct Eng 2019;145(1):05018002.

[27] Terzioglu T, Karthik MM, Hurlebaus S, Hueste MBD, Maack S, Woestmann J, et al. Nondestructive evaluation of grout defects in internal tendons of posttensioned girders. NDT E Int 2018;99:23–35.

[28] Weischedel HR. Magnetic flux leakage inspection of wire ropes. NDT Technologies, Inc.; 2003.

[29] Mehrabi AB. In-service evaluation of cable-stayed bridges, overview of available methods and findings. J. Bridge Eng. 2006;11(6).

[30] Sun Z, Li G, Geng S. Study on stayed-cable health monitoring. In: Proc., Intelligence Computation and Evolutionary Computation, Berlin; 2013.